

Optical spin-to-orbital angular momentum conversion in structured optical fields

Yang Zhao(赵阳), Cheng-Xi Yang(阳成熙), Jia-Xi Zhu(朱家玺), Feng Lin(林峰), Zhe-Yu Fang(方哲宇), Xing Zhu(朱星)

Citation: Chin. Phys. B . 2020, 29(6): 067301 . **doi:** 10.1088/1674-1056/ab862a
Journal homepage: http://cpb.iphy.ac.cn; http://iopscience.iop.org/cpb

What follows is a list of articles you may be interested in

Selective excitation of multipolar surface plasmon in a graphene-coated dielectric particle by Laguerre Gaussian beam

Yang Yang(杨阳), Guanghua Zhang(张光华), Xiaoyu Dai(戴小玉)

Chin. Phys. B . 2020, 29(5): 057302 . **doi:** 10.1088/1674-1056/ab7e97

Research progress of femtosecond surface plasmon polariton

Yulong Wang(王玉龙), Bo Zhao(赵波), Changjun Min(闵长俊), Yuquan Zhang(张聿全), Jianjun Yang(杨建军), Chunlei Guo(郭春雷), Xiaocong Yuan(袁小聪)

Chin. Phys. B . 2020, 29(2): 027302 . **doi:** 10.1088/1674-1056/ab6717

Strong coupling in silver-molecular J-aggregates-silver structure sandwiched between two dielectric media

Kunwei Pang(庞昆维), Haihong Li(李海红), Gang Song(宋钢), Li Yu(于丽)

Chin. Phys. B . 2019, 28(12): 127301 . **doi:** 10.1088/1674-1056/ab4fda

Plasmon reflection reveals local electronic properties of natural graphene wrinkles

Runkun Chen(陈闰堃), Cui Yang(杨翠), Yuping Jia(贾玉萍), Liwei Guo(郭丽伟), Jianing Chen(陈佳宁)

Chin. Phys. B . 2019, 28(11): 117302 . **doi:** 10.1088/1674-1056/ab46a2

Remote excitation and remote detection of a single quantum dot using propagating surface plasmons on silver nanowire

Li Qiang, Wei Hong, Xu Hong-Xing

Chin. Phys. B . 2014, 23(9): 097302 . **doi:** 10.1088/1674-1056/23/9/097302

Optical spin-to-orbital angular momentum conversion in structured optical fields*

Yang Zhao(赵阳)[1], Cheng-Xi Yang(阳成熙)[1], Jia-Xi Zhu(朱家玺)[1], Feng Lin(林峰)[1,†], Zhe-Yu Fang(方哲宇)[1,2,3,4,‡], and Xing Zhu(朱星)[1,2,4]

[1] *State Key Laboratory for Mesoscopic Physics, School of Physics, Peking University, Beijing* 100871, *China*
[2] *Center for Nanoscale Science and Technology, Academy for Advanced Interdisciplinary Studies, Peking University, Beijing* 100871, *China*
[3] *Collaborative Innovation Center of Quantum Matter, Beijing* 100871, *China*
[4] *National Center for Nanoscience and Technology, Beijing* 100190, *China*

(Received 3 March 2020; revised manuscript received 31 March 2020; accepted manuscript online 3 April 2020)

We investigate the dynamic quantities: momentum, spin and orbital angular momenta (SAM and OAM), and their conversion relationship in the structured optical fields at subwavelength scales, where the spin–orbit interaction (SOI) plays a key role and determines the behaviors of light. Specifically, we examine a nanostructure of a Ag nanoparticle (Ag NP) attached on a cylindrical Ag nanowire (Ag NW) under illumination of elliptically polarized light. These dynamic quantities obey the Noether theorem, i.e., for the Ag nanoparticle with spherical symmetry, the total angular momentum consisting of SAM and OAM conserves; for the Ag NW with translational symmetry, the orbital momentum conserves. Meanwhile, the spin-to-orbital angular momentum conversion is mediated by SOI arising from the spatial variation of the optical potential. In this nanostructure, the conservation of momentum imposes a strict restriction on the propagation direction of the surface plasmon polaritons along the Ag NW. Meanwhile, the orbital momentum is determined by the polarized properties of the excitation light and the topography of the Ag NP. Our work offers insights to comprehend the light behaviors in the structured optical fields in terms of the dynamic quantities and benefits to the design of optical nano-devices based on interactions between spin and orbital degrees of freedom.

Keywords: orbital angular momentum, spin angular momentum, spin–orbit interaction of light, silver nanowire

PACS: 73.20.Mf, 78.20.Bh, 78.67.Uh, 78.67.Bf **DOI:** 10.1088/1674-1056/ab862a

1. Introduction

Nowadays, the spin–orbit interaction (SOI) of light has attracted great attention in optics, owing to its fundamental physical significance and potential applications in novel photonic devices.[1–17] It turns out that most of conventional optical processes, such as propagation, reflection, focusing, scattering, are associated with the SOI,[5,7,18,19] although they have very weak manifestation, and are often neglected in traditional macroscopic geometrical optics. For example, in the spin Hall effects of light,[4,13,20] the SOI deviates photons with opposite spins–left-handed or right-handed circularly polarized light (LCP or RCP)–propagating in different directions with a transverse subwavelength shift when they are incident on the interface of different media. While in nano-optics, by engineering SOI using metamaterials, geometrical phases, and plasmonic nanostructures at subwavelength scales, it was demonstrated that spin-related optical phenomena induced by SOI are more distinct than those occurred in macroscopic optics. In the subwavelength-sized structured optical fields, the propagation direction of light varies rapidly with the variation of the medium permittivity and permeability, which leads to the spin change due to the correlation of the electric field $\boldsymbol{E}$ and the wavevector $\boldsymbol{k}$ by the transversality condition $\boldsymbol{k}\cdot\boldsymbol{E}(\boldsymbol{k})=0$. In most cases, the SOI effects are described in terms of the electromagnetic field quantities, which represent the wave properties of light. When concerning the SOI, it is also reasonable to use the dynamic quantities, such as momentum, spin and orbital angular momenta (SAM and OAM), to describe the behaviors of light in structured optical fields, which can better clarify the physical processes as does in the electron counterparts. Recently, Bliokh *et al.*[21,22] gave a detailed theoretical derivation about the representation of these dynamic quantities in the canonical Minkowski approach,[23] which is very valid to describe structured optical fields in dispersive inhomogeneous media. Therefore it is of significance to present a specific structured optical field for revealing the behaviors of the dynamic quantities.

Here we present a prototypical nanostructure constructed by a spherical Ag nanoparticle (Ag NP) attached on a cylindrical Ag nanowire (Ag NW) under illumination of elliptically polarized light. A clear picture shows that the conversion of spin-to-orbital angular momentum occurs through the

*Project supported by the National Key R&D Program of China (Grant Nos. 2017YFA0205700, 2015CB932403, and 2017YFA0206000) and the National Natural Science Foundation of China (Grant Nos. 21790364, 11374023, 61422501, 11674012, 61176120, 61378059, 6097701, and 61521004).

†Corresponding author. E-mail: linf@pku.edu.cn
‡Corresponding author. E-mail: zhyfang@pku.edu.cn

© 2020 Chinese Physical Society and IOP Publishing Ltd

SOI arising from the spatial variation of the optical potential. Due to the symmetry of the nanostructure, the total angular momentum consisting of SAM and OAM conserves under the spherical symmetry; the orbital momentum conserves under the translational symmetry. The conservation of momentum imposes a strict restriction on the propagation direction of the surface plasmon polaritons along the Ag NW.

2. Results and discussion

In subwavelength-scale structured optical fields, the Dirac-like form of Maxwell equations is more appropriate to describe the dynamical behaviors of light, which is[6]

$$c(\hat{\alpha}\cdot\hat{p})\Phi+\hat{\beta}V\Phi=\mathrm{i}\frac{\partial}{\partial t}\Phi, \tag{1}$$

where the term in the left hand side of this equation corresponds to Hamiltonian H; c is the speed of light in vacuum; Φ is the complex two-level state vector of the electric and magnetic fields, $\Phi=\sqrt{(4\omega)^{-1}}\left[\sqrt{\varepsilon_0}\boldsymbol{E}\sqrt{\mu_0}\boldsymbol{H}\right]^{\mathrm{T}}$; $\hat{\alpha}_i$ $(i=1,2,3)$ and $\hat{\beta}$ are the Dirac matrices, $\hat{\alpha}_i$ is the spin-1 Pauli operator, representing the photonic SAM; $\hat{p}$ is the momentum operator $-\mathrm{i}\nabla$; V is the optical potential contributed by the optical media, $V=\omega\begin{pmatrix}1-\varepsilon & 0\\ 0 & 1-\mu\end{pmatrix}$. In analogy with the electric potential, the gradient of which leads to the electric SOI, the optical SOI described by the term $\hat{\alpha}\cdot\hat{p}$ in this equation arises from the spatial variation of V, which at the subwavelength scale leads to the greater magnitude of the gradient of V. The large gradient of V produces a non-negligible SOI related term if equation (1) is expanded in a specific physical system, which makes a significant spin-to-orbital conversion.

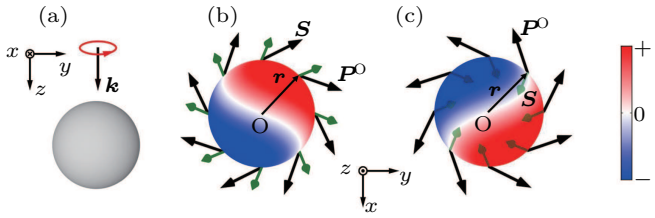


Fig. 1. (a) Schematic of a spherical Ag nanoparticle with the radius of 100 nm under illumination of circularly polarized light. The incident light propagates along the z-axis, the wavelength is 671 nm. Under (b) LCP and (c) RCP illumination, $\boldsymbol{P}^{\mathrm{O}}$ and $\boldsymbol{S}$ of the scattering light displayed at the x–y plane crossing the spherical surface. The origin locates at the center of the sphere. $\boldsymbol{r}$ is the radial vector. The red color in the sphere represents the positive charge distribution, and the blue the negative charge distribution. The black (green) arrows indicate the direction of $\boldsymbol{P}^{\mathrm{O}}$ ($\boldsymbol{S}$).

Based on Eq. (1), the local dynamical quantities of the electromagnetic field involved can be derived, including the orbital (or canonical) momentum density $\boldsymbol{P}^{\mathrm{O}}$, orbital angular momentum density $\boldsymbol{L}$, and spin angular momentum density $\boldsymbol{S}$[21,22]

$$\boldsymbol{P}^{\mathrm{O}}=\langle\Phi|-\mathrm{i}\nabla|\Phi\rangle=\frac{1}{4\omega}\mathrm{Im}\left[\boldsymbol{E}^{*}\cdot(\nabla)\boldsymbol{E}+\boldsymbol{H}^{*}\cdot(\nabla)\boldsymbol{H}\right], \tag{2}$$

$$\boldsymbol{L}=\boldsymbol{r}\times\boldsymbol{P}^{\mathrm{O}}, \tag{3}$$

$$\boldsymbol{S}=\langle\Phi|\hat{\alpha}|\Phi\rangle=\frac{1}{4\omega}\mathrm{Im}\left[\boldsymbol{E}^{*}\times\boldsymbol{E}+\boldsymbol{H}^{*}\times\boldsymbol{H}\right]. \tag{4}$$

Firstly, we consider a spherical Ag nanoparticle with the radius of 100 nm under illumination of a circularly polarized light, as schematically shown in Fig. 1(a). All simulations are based on finite element method (FEM), using commercial software package COMSOL Multiphysics. The incident excitation is described by a Gaussian beam (wavelength $\lambda=671$ nm, waist $\omega_0=1.2$ μm). The optical constants for Ag are taken from Johnson's work.[24] The simulations use the scattering boundary conditions. At the wavelength 671 nm of the incident light, the localized surface plasmon resonance (LSPR) occurs for this Ag NP, and the resonance scattering light carrying SAM and OAM takes on the SOI characteristics, especially in the near field. Figures 1(b) and 1(c) show the $\boldsymbol{P}^{\mathrm{O}}$ and $\boldsymbol{S}$ distributions around the x–y cross section of the sphere under illumination of left-handed and right-handed circularly polarized light, respectively. Considering the spherical symmetry of the system, $\boldsymbol{P}^{\mathrm{O}}$ and $\boldsymbol{S}$ uniformly clockwise and anticlockwise surround the spherical surface in the near field, respectively. In terms of the definition of OAM in Eq. (1), if taking the spherical center as the coordinate origin, we can obtain a value of $\boldsymbol{L}$. The helicity of $\boldsymbol{L}$ has the same direction compared with the incident light SAM. Due to the difference between the optical dielectric medium of the Ag NP and air, there exists a optical potential difference, $\boldsymbol{V}(\boldsymbol{r})=\omega[1-\varepsilon(\boldsymbol{r})]$, which results in the SOI effect. Here, the polarizability α of the spherical Ag NP can be considered to be isotropic and uniform, therefore the optical potential $\boldsymbol{V}(\boldsymbol{r})$ is spherically symmetric. The total AM density $\boldsymbol{J}$ in this system is written as

$$\boldsymbol{J}=\boldsymbol{L}+\boldsymbol{S}=\boldsymbol{r}\times\boldsymbol{P}^{\mathrm{O}}+\boldsymbol{S}. \tag{5}$$

Taking into account the Hamiltonian H with spherically symmetric $\boldsymbol{V}(\boldsymbol{r})$, we have $[\boldsymbol{J},H]=0$, i.e., $\boldsymbol{J}$ commutes with H, which means that $\boldsymbol{J}$ is conserved. In the incident light, there is only $\boldsymbol{S}$, with $\boldsymbol{L}=0$. Therefore, the OAM in the scattering light is converted from the incident SAM by means of the SOI.

As schematically shown in Fig. 2(a), the Ag NP is placed on the middle of a cylindrical Ag nanowire , which has a radius of 60 nm and a length of 6 μm. The gap between them is 5 nm. Under illumination of a circularly polarized Gaussian beam in z direction, from the medium polarization point of view, the opposite charges generate at the two sides of the small gap, which leads to a very strong field enhancement, called gap plasmon resonance that is much strong than the LSPR for the single Ag NP.[25] From the dynamic point of view, the optical potential undergoes a drastic variation in the very small gap space, which results in a giant SOI effect, and the very large $\boldsymbol{P}^{\mathrm{O}}$ appears in the gap. As shown in Figs. 2(b_1) (LCP) and 2(c_1) (RCP), $\boldsymbol{P}^{\mathrm{O}}$ in the gap is much larger than that at other

parts around the Ag NP, the direction of which depends on the helicity of the incident light. Qualitatively, $\boldsymbol{P}^{\mathrm{O}}$ is also much larger than the corresponding $\boldsymbol{S}$, which means that a greater amount of the incident SAM is converted to OAM due to the strong SOI effect. Define δ the angle between $\boldsymbol{P}^{\mathrm{O}}$ and the NW axis ($+y$); $\delta = 171.1°$ for LCP [Fig. 2(b$_2$)], and $\delta = 8.9°$ for RCP [Fig. 2(c$_2$)], which are almost opposite in direction. Due to the strong gap plasmon resonance, the coupling between Ag NW and Ag NP occurs in the gap, which excites the surface plasmon polaritons (SPPs) propagating along the Ag NW. The direction of the SPPs depends on $\boldsymbol{P}^{\mathrm{O}}$ in the gap.

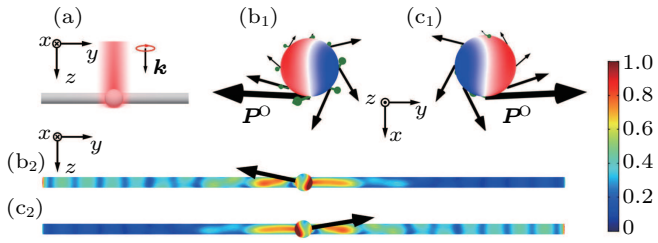


Fig. 2. (a) Schematic of a spherical Ag nanoparticle with the radius of 100 nm attached on a cylindrical Ag nanowire with the radius of 60 nm and the length of 6 μm under illumination of circularly polarized light. The incident light propagates along the z-axis, the wavelength is 671 nm. Under (b$_1$), (b$_2$) LCP and (c$_1$), (c$_2$) RCP illumination, $\boldsymbol{P}^{\mathrm{O}}$ and $\boldsymbol{S}$ of the scattering light displayed at the x–y and y–z planes crossing the spherical surface. The direction of $\boldsymbol{P}^{\mathrm{O}}$ is relative to the Ag NW axis. The color in the Ag NW represents the electric field of SPPs propagating along the NW. The intensity meter is shown at the right.

Only considering the Ag NW, it is cylindrically symmetric, the optical potential presents the form of $\boldsymbol{V}(\rho)$, where ρ is the polar coordinate in x–z plane. In y-direction along the NW, $\boldsymbol{V}(\rho)$ is translationally invariance. Taking into account the Hamiltonian H with cylindrically symmetric $\boldsymbol{V}(\rho)$, we have $\left[\boldsymbol{P}_y^{\mathrm{O}}, H\right] = 0$, i.e., $\boldsymbol{P}_y^{\mathrm{O}}$ is conserved. The direction of $\boldsymbol{P}^{\mathrm{O}}$ in the gap is more close to the axis of the cylindrical Ag NW ($+y$ or $-y$), the more amount of excited SPPs propagates in this Ag NW direction. In Figs. 2(b$_2$) and 2(c$_2$), respectively, the greater amount of SPPs propagate along $-y$ direction (left side of the NW) for LCP illumination, while the greater amount of SPPs propagate along $+y$ direction (right side of the NW) for RCP illumination.

As mentioned above, the $\boldsymbol{P}^{\mathrm{O}}$ direction in the gap is mainly governed by the incident light helicity. By changing the ratio of different helicities in the incident light, we can vary the $\boldsymbol{P}^{\mathrm{O}}$ direction, and then adjust the amount of SPPs propagating along one side of the Ag NW. For this purpose, we use elliptically polarized light to illuminate the above Ag NP and NW system. The complex electric field of this incident light can be written as

$$\boldsymbol{E}(\boldsymbol{r}) = E_0 \left(\bar{\boldsymbol{x}} \sin\frac{\theta}{2} + \bar{\boldsymbol{y}} \cos\frac{\theta}{2} \mathrm{e}^{\mathrm{i}\phi} \right) \mathrm{e}^{\mathrm{i}kz}, \tag{6}$$

where E_0 is the light amplitude, the angles θ and ϕ determine the polarization state.

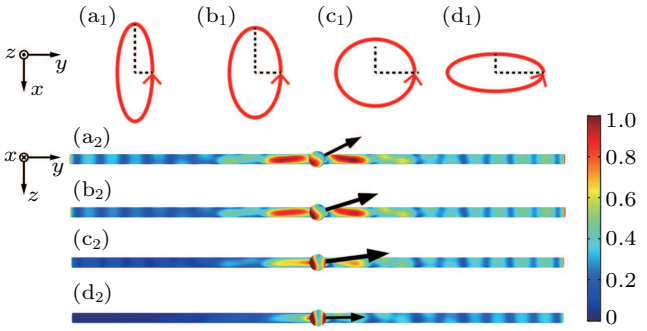


Fig. 3. The incident light is elliptically polarized, with (a$_1$) (θ, ϕ) = (140°, 90°); (b$_1$) (120°, 90°); (c$_1$) (60°, 90°); (d$_1$) (42°, 90°). (a$_2$), (b$_2$), (c$_2$), and (d$_2$) show the corresponding direction of $\boldsymbol{P}^{\mathrm{O}}$ relative to the Ag NW axis. The color in the Ag NW represents the electric field of SPPs propagating along the NW.

Through simulation and comparison, we choose four different elliptically polarized light, as shown in Figs. 3(a$_1$), 3(b$_1$), 3(c$_1$), and 3(d$_1$), $(\theta, \phi) = (140°, 90°)$; (120°, 90°); (60°, 90°); (42°, 90°), with gradually increasing RCP component and decreasing LCP component in the incident elliptically polarized light. As shown in Figs. 3(a$_2$), 3(b$_2$), 3(c$_2$), and 3(d$_2$), the resultant $\boldsymbol{P}^{\mathrm{O}}$ is the vector sum of $\boldsymbol{P}_{\mathrm{L}}^{\mathrm{O}}$ induced by the LCP component and $\boldsymbol{P}_{\mathrm{R}}^{\mathrm{O}}$ induced by the RCP component. At (θ, ϕ) = (42°, 90°) [Fig. 3(d)], $\boldsymbol{P}^{\mathrm{O}}$ is almost parallel to the Ag NW with $\delta = 4.8°$, pointing to the right side of the NW. Therefore, the maximum amount of SPPs propagating to the right side of the Ag NW can be obtained. Here, we define the directionality of SPPs on the Ag NW as

$$D = \frac{|c_+| - |c_-|}{|c_+| + |c_-|}, \tag{7}$$

where c_+ and c_- correspond to the average power flows along the right side and left side of the Ag NW, respectively. The D values are 0.26, 0.40, 0.83, and 0.90, corresponding to the four different elliptically polarized incident light, respectively. In a similar way, by increasing the LCP component and decreasing the RCP component in the incident elliptically polarized light, the opposite result can be obtained, which is the maximum amount of SPPs propagating to the left side of the Ag NW.

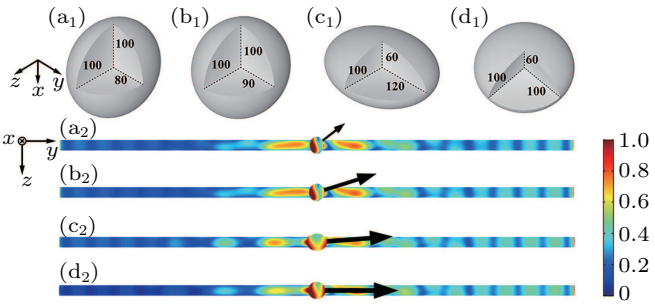


Fig. 4. The Ag NPs on the middle of NW are ellipsoids. (a$_1$), (b$_1$), (c$_1$), and (d$_1$) are four different ellipsoids, with the three semi-axes labeled on each ellipsoid, the unit is nm. (a$_2$), (b$_2$), (c$_2$), and (d$_2$) show the direction of $\boldsymbol{P}^{\mathrm{O}}$ relative to the Ag NW axis. The color in the Ag NW represents the electric field of SPPs propagating along the NW.

The topography of the Ag NP can also affect the direction of $\boldsymbol{P}^{\mathrm{O}}$ in the gap. Without loss of generality, the Ag NP

is changed from the aforementioned sphere to an ellipsoid, as shown in Fig. 4. Under RCP illumination, the polarization $\boldsymbol{P}$ of the ellipsoid can be expressed as

$$\boldsymbol{P} = \bar{\alpha}\boldsymbol{E}_{\text{inc}} = \begin{pmatrix} \alpha_x & 0 & 0 \\ 0 & \alpha_y & 0 \\ 0 & 0 & \alpha_z \end{pmatrix} \begin{pmatrix} E_0 \\ \mathrm{i}E_0 \\ 0 \end{pmatrix} = \begin{pmatrix} \alpha_x E_0 \\ \mathrm{i}\alpha_y E_0 \\ 0 \end{pmatrix}, \quad (8)$$

where E_0 is the incident electric field amplitude, α_i is the polarizability in the i $(= x, y, z)$ direction. Due to the anisotropic polarizability for the ellipsoid, i.e., $\alpha_x \neq \alpha_y$, the incident RCP light transforms into elliptically polarized radiation. Therefore, as the aforementioned analysis, $\delta = 40.0°$, 17.8°, 4.2°, 2.4°; $D = 0.33$, 0.49, 0.50, 0.84 for the different ellipsoids, as shown in Figs. 4(a$_2$), 4(b$_2$), 4(c$_2$), and 4(d$_2$), respectively.

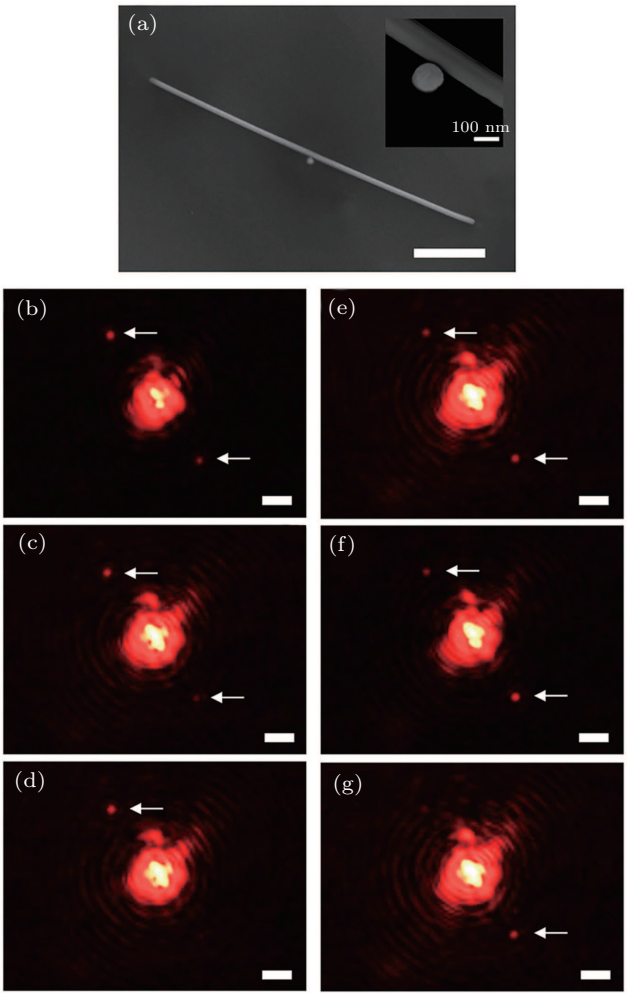


Fig. 5. (a) Scanning electron microscope image of a Ag NP attached on almost the middle of a Ag NW. The inset shows the shape of the Ag NP. The excited light is incident on the Ag NP. (b)–(g) Optical micrographs of the scattering light at the two ends of the NW under different polarized conditions. The polarized angles (θ, ϕ) are (b) (−140°, 90°), (c) (−90°, 90°), (d) (−41°, 90°), (e) (140°, 90°), (f) (90°, 90°), (g) (41°, 90°). The arrows indicate the scattering light spots. The scale bars indicate 2 μm.

In experiments, chemically synthesized Ag NWs and NPs were deposited simultaneously on a silicon substrate. By seeking under scanning electron microscope, we obtained a desired sample showing that a NP adhered on almost the middle of a NW [Fig. 5(a)], where the NP roughly has a spherical shape with the diameter of about 120 nm [inset of Fig. 5(a)], the NW is 140 nm in diameter and 10.3 μm in length. We focused a laser beam with the wavelength of 671 nm through a 100× objective (N.A. = 0.9) on the Ag NP. The helicity of the elliptically polarized light was obtained by adjusting a polarizer and a quarter-wave plate mounted in the light path. The exact values of the helicity were determined by a Thorlabs TXP5004 polarimeter. The excited SPPs propagated along the NW, and were converted back to free-space scattering light at the two distal ends which were collected by the same objective; and the optical images were recorded by a CCD detector mounted on the optical microscope. As shown in Figs. 5(b)–5(d), the elliptically polarized angles (θ, ϕ) are altered from (−140°, 90°), (−90°, 90°) to (−41°, 90°), the light spots indicated by the arrows become gradually weak at the lower end of the NW, indicating that $\boldsymbol{P}^{\text{O}}$ is more and more pointing to the upper end. As expected, by changing the helicity sign of the elliptically polarized incident light [Figs. 5(e)–5(g)], the angles are $(\theta, \phi) = (140°, 90°)$, (90°, 90°), and (41°, 90°), the light spots at the upper end of the NW become gradually weak. The experiment demonstrates that the helicity of the polarized light is able to control the direction of the surface plasmon polaritons on the Ag NW, which is consistent with the simulation results.

3. Conclusion

In summary, we have investigated the evolution of momentum, spin and orbital angular momenta, and their SOI in the structured optical fields that are creased by a spherical Ag NP attached on a cylindrical Ag NW. It is found that in the case of a spherical symmetric Ag NP, the conservation of angular momenta (including SAM and OAM) is obeyed; in the case of a translational symmetric Ag NW, the conservation of momentum is obeyed. Spin-to-momentum conversion is mediated by the SOI which arises from the spatial variation of the optical potential. The helicity of the polarized light is able to control the direction of the orbital momentum $\boldsymbol{P}^{\text{O}}$ at the gap between the Ag NP and NW, which can govern the propagation direction of SPPs excited on the Ag NW based on the conservation of momentum. The behavior analysis of the dynamic quantities in the structured optical fields offers a new approach to assist the design of optical nano-devices.

References

[1] Bliokh K Y, Smirnova D and Nori F 2015 *Science* **348** 1448
[2] High A A, Devlin R C, Dibos A, Polking M, Wild D S, Perczel J, de Leon N P, Lukin M D and Park H 2015 *Nature* **522** 192
[3] Kapitanova P V, Ginzburg P, Rodriguez-Fortuno F J, Filonov D S, Voroshilov P M, Belov P A, Poddubny A N, Kivshar Y S, Wurtz G A and Zayats A V 2014 *Nat. Commun.* **5** 3226
[4] Ling X, Zhou X, Huang K, Liu Y, Qiu C W, Luo H and Wen S 2017 *Rep. Prog. Phys.* **80** 066401

[5] O'Connor D, Ginzburg P, Rodriguez-Fortuno F J, Wurtz G A and Zayats A V 2014 *Nat. Commun.* **5** 5327
[6] Pan D, Wei H, Gao L and Xu H 2016 *Phys. Rev. Lett.* **117** 166803
[7] Petersen J, Volz J and Rauschenbeutel A 2014 *Science* **346** 67
[8] Slobozhanyuk A P, Poddubny A N, Sinev I S, Samusev A K, Yu Y F, Kuznetsov A I, Miroshnichenko A E and Kivshar Y S 2016 *Laser Photon. Rev.* **10** 656
[9] Sukhov S, Kajorndejnukul V, Naraghi R R and Dogariu A 2015 *Nat. Photon.* **9** 809
[10] Tsesses S, Cohen K, Ostrovsky E, Gjonaj B and Bartal G 2019 *Nano Lett.* **19** 4010
[11] Vallone G, D'Ambrosio V, Sponselli A, Slussarenko S, Marrucci L, Sciarrino F and Villoresi P 2014 *Phys. Rev. Lett.* **113** 060503
[12] Wang Y, Xu Y, Feng X, Zhao P, Liu F, Cui K, Zhang W and Huang Y 2016 *Opt. Lett.* **41** 1478
[13] Yin X, Ye Z, Rho J, Wang Y and Zhang X 2013 *Science* **339** 1405
[14] Zhou J, Qian H, Hu G, Luo H, Wen S and Liu Z 2018 *ACS Nano* **12** 82
[15] Gong S H , Alpeggiani F, Sciacca B, Garnett E C and Kuipers L 2018 *Science* **359** 443
[16] Guo Q, Fu T, Tang J, Pan D, Zhang S and Xu H 2019 *Phys. Rev. Lett.* **123** 183903
[17] Yang L, Jie R, HaiTao J, Yong S and Hong C 2017 *Acta Phys. Sin.* **66** 22 (in Chinese)
[18] Donato M, Hernandez J, Mazzulla A, Provenzano C, Saija R, Sayed R, Vasi S, Magazzù A, Pagliusi P and Bartolino R 2014 *Nat. Commun.* **5** 3656
[19] Zhang T, Mahdy M R C, Liu Y, Teng J H, Lim C T, Wang Z and Qiu C W 2017 *ACS Nano* **11** 4292
[20] Onoda M, Murakami S and Nagaosa N 2004 *Phys. Rev. Lett.* **93** 083901
[21] Bliokh K Y, Bekshaev A Y and Nori F 2017 *Phys. Rev. Lett.* **119** 073901
[22] Bliokh K Y, Kivshar Y S and Nori F 2014 *Phys. Rev. Lett.* **113** 033601
[23] Soper D E 1976 *Classical Field Theory* (New York: Wiley)
[24] Johnson P B and Christy R W 1972 *Phys. Rev. B* **6** 4370
[25] Baumberg J J, Aizpurua J, Mikkelsen M H and Smith D R 2019 *Nat. Mater.* **18** 668